

RESEARCH ARTICLE | APRIL 21 2023

Unraveling the decarboxylation dynamics of the fluorescein dianion with fragment action spectroscopy

J. A. Gibbard and J. R. R. Verlet

Jemma A. Gibbard  ; Jan R. R. Verlet



J. Chem. Phys. 158, 154306 (2023)

<https://doi.org/10.1063/5.0144851>



CrossMark

Articles You May Be Interested In

Primary reactions in crystalline Rochelle salt studied by pulse radiolysis and EPR spectroscopy. The decarboxylation of the acyloxy radical ion

J. Chem. Phys. (August 2008)

Fluorescein by XPS

Surface Science Spectra (September 1992)

Influence of the repulsive Coulomb barrier on photoelectron spectra and angular distributions in a resonantly excited dianion

J. Chem. Phys. (August 2013)



Time to get excited.
Lock-in Amplifiers – from DC to 8.5 GHz

[Find out more](#)

 Zurich
Instruments

Unraveling the decarboxylation dynamics of the fluorescein dianion with fragment action spectroscopy

Cite as: J. Chem. Phys. 158, 154306 (2023); doi: 10.1063/5.0144851

Submitted: 1 February 2023 • Accepted: 6 April 2023 •

Published Online: 21 April 2023



View Online



Export Citation



CrossMark

Jemma A. Gibbard^{a)}  and Jan R. R. Verlet 

AFFILIATIONS

Department of Chemistry, Durham University, Durham DH1 3LE, United Kingdom

^{a)} Author to whom correspondence should be addressed: jemma.gibbard@durham.ac.uk

ABSTRACT

The decarboxylation dynamics of the doubly deprotonated fluorescein dianion, Fl^{2-} , are investigated by recording fragment action spectra for the anion, Fl^- , and its decarboxylated analog, Fl-CO_2^- , using a new reflectron secondary mass spectrometer. The formation of the anion, Fl^- , is directly investigated by photoelectron imaging. The Fl^- and Fl-CO_2^- action spectra indicate that, for $\lambda < 400$ nm, one-photon dissociative photodetachment, i.e., simultaneous decarboxylation and electron loss, competes with photodetachment, whereas for $\lambda > 400$ nm, decarboxylation only proceeds following electron loss via a sequential two-photon process. The primary decarboxylation pathway is the ready loss of CO_2 from the relatively short-lived intermediate excited state, $\text{Fl}^-[\text{D}_1]$, which is formed by electron loss from the dianion via resonant tunneling through the repulsive Coulomb barrier associated with a high-lying excited dianion state, $\text{Fl}^{2-}[\text{S}_2]$.

© 2023 Author(s). All article content, except where otherwise noted, is licensed under a Creative Commons Attribution (CC BY) license (<http://creativecommons.org/licenses/by/4.0/>). <https://doi.org/10.1063/5.0144851>

I. INTRODUCTION

Fluorescein is a dye and fluorescent tracer, and many of its applications exploit its intense solution-phase fluorescence.¹ Several charged and neutral pH dependent forms of fluorescein exist in the solution phase, including a doubly deprotonated dianion (Fl^{2-}), which has a fluorescence maximum at 500 nm, corresponding to radiative relaxation from $\text{S}_1 \rightarrow \text{S}_0$.^{1,2} While the fluorescence quantum yield in solution is very high, previous studies have indicated that Fl^{2-} does not fluoresce in the gas phase; instead, S_1 decays via electron loss.^{2,3} Decarboxylation of the carboxylate group of Fl^{2-} may also be favorable, given the high thermodynamic stability of CO_2 , particularly if the Fl^- radical anion that is formed following electron loss from the dianion has a carboxyl radical character.^{4,5} In fact, multiple photon excitation of Fl^{2-} in the infrared (IR) (via irradiation with a CO_2 laser) and collisionally induced dissociation (CID) of Fl^{2-} were found to exclusively produce decarboxylation with electron loss (i.e., $\text{Fl-CO}_2^- + \text{e}^- + \text{CO}_2$), in contrast to excitation in the visible, where electron loss was the dominant channel (i.e., $\text{Fl}^- + \text{e}^-$).² Therefore, the mechanism for decarboxylation, as well as the role of excited states in mediating the electron

loss and decarboxylation dynamics of Fl^{2-} , remains unclear. In this manuscript, we present fragment action spectroscopy of Fl^{2-} in the gas-phase between $\lambda = 260\text{--}600$ nm in order to gain insight into the competition between electron and CO_2 loss from Fl^{2-} .

Dianions, such as Fl^{2-} , are characterized by the balance of long range repulsive forces and short range attractive forces, which constitute the repulsive Coulomb barrier (RCB).^{3,6–11} There is a multitude of RCBs associated with a dianion corresponding to individual rovibronic states of the parent species and linked to distinct product channels, whether that be electron or anion loss channels.^{12,13} Therefore, each RCB forms a barrier to the loss of low kinetic energy electrons or anionic fragments. One key distinction between the study of electron loss and anionic dissociation processes of dianions is the relative prevalence of tunneling through a specific RCB. Resonant and non-resonant electron tunneling through an RCB has been observed for many dianions, on account of the low mass of the electron.^{14–17} In contrast, anionic fragmentation of dianions has only been observed as an “over-the-barrier” process.^{13,18}

Experimentally, the properties of dianions and their electronic RCBs have been effectively studied by photoelectron spectroscopy, where a characteristic low electron kinetic energy (eKE) cutoff is

observed in the photoelectron spectra at the minimum height of the RCB.^{18–22} Electron loss via tunneling has been observed by the presence of photoelectrons below the cutoff, and these features are often spectrally characterized by a peak at fixed eKE, which is invariant with photon energy.^{3,12,23} Photodissociation spectroscopy has also been used to study anion loss from dianions, in particular for IrBr_6^{2-} , where the minimum height of the RCB to fragmentation has been reported from the kinetic energy release of the Br^- fragment.^{13,18,24,25} The groups of Weber and Kappes have used reflectron time-of-flight mass spectrometry to record fragment action spectra,^{18,25,26} while other methodologies, such as the collisional activation or laser excitation of dianions in a quadrupole trap or electrostatic ion storage rings, have also been used to study polyanion dissociation dynamics.^{2,13,24}

Previous work in our group has studied the photodetachment dynamics of Fl^{2-} using frequency-resolved photoelectron imaging.^{3,12,27} Unusual and rich photodetachment dynamics were observed, with electron loss occurring via several distinct resonant tunneling pathways that are associated with different mediating dianion states, RCBs and final anion states.¹² While photoelectron spectroscopy can yield a detailed picture of the electron loss dynamics, once the electron has been lost, this methodology is blind to any subsequent dynamical process, such as dissociation. This is the case for Fl^{2-} , where CO_2 loss has been observed in conjunction with electron loss under specific experimental circumstances.² So how do such dissociation dynamics take place and can this be reconciled with the electron dynamics? Commonly observed processes involve electron loss from a carboxylate anion, leading to rapid decarboxylation of a transiently formed carboxyl radical via a repulsive potential energy surface.^{4,5,28–30} However, it is unclear if the Fl^- formed following electron loss from Fl^{2-} would have carboxyl radical character and be expected to undergo a similar repulsive dissociation. Additionally, the photodetachment dynamics indicate that at higher photon energies, new tunneling pathways compete, which leads to the formation of a highly internally excited Fl^- , both electronic and/or vibrational. The role of vibrational excitation may be important if CO_2 loss occurs via a ground state dissociation, while different electronic states in the anionic product may have different dissociation dynamics. In this manuscript, we build on the previously reported photoelectron imaging studies, which focused on the nature of the RCB, to unravel the decarboxylation dynamics of Fl^{2-} by the application of fragment action spectroscopy.^{3,12}

II. METHODS

The action spectrum of a fragment ion cannot be recorded using linear time-of-flight methods as, to a first approximation, all of the photoproducts have the same velocity as the parent species, making it challenging to separate the time-of-flight of the fragment ions from the parent dianions. In order to overcome this limitation, a secondary mass spectrometer consisting of a reflectron was introduced, which acts as an electrostatic kinetic energy filter, in order to temporally separate the charged photoproducts with different $\frac{m}{z}$ ratios.^{31,32} We can study both the photodetachment (different z) and photodissociation (different m and sometimes z) of dianions using this methodology.

The ion beam and light source used in this apparatus are the same as for previous photoelectron imaging experiments and have

been described in detail elsewhere.^{33,34} Briefly, Fl^{2-} was produced using electrospray ionization of a 1 mM solution of sodium fluorescein in methanol. The dianions entered the vacuum via a capillary and were guided and trapped by a series of radio frequency ring electrodes, before acceleration at -1.5 keV using a Wiley–Maclaren time-of-flight mass spectrometer. The dianions of interest were mass selected by time-of-flight at the intersection of the ion beam with the nanosecond tunable output of a Nd:YAG pumped optical parametric oscillator, which induces photochemistry in Fl^{2-} . Likely, photo products include photoelectrons, which can be studied by photoelectron imaging,^{19,20} and anions produced via electron loss, dissociation, or a combination of both.

The new detector region, including the reflectron secondary mass spectrometer, is shown schematically in Fig. 1. After the interaction of laser light and Fl^{2-} , any product anions, including Fl^- (blue), continue along the same beam axis as Fl^{2-} (red), past a grounded detector and deflector, and into the reflectron. As the kinetic energy of the dianion ($\frac{m}{z} = \frac{m_{\text{Fl}^{2-}}}{2} = 165$ amu) is half that of the anion ($\frac{m}{z} = m_{\text{Fl}^-} = 330$ amu), the two ion packets can be temporally separated by the behavior of the reflectron as a kinetic energy filter. The reflectron consists of a grounded front plate, followed by a resistive glass tube (15 cm long) that is biased at either end (front plate, $V_f = -700$ V and mirror plate, $V_m = -3500$ V). As the kinetic energy of the anion product is twice as large as the dianion, the mirror voltage of the reflectron must be more than twice the beam energy of the dianion in order to reflect the anions for detection. This is shown in Fig. 1 by the Fl^{2-} (red) and Fl^- (blue) ion paths, where the flight distance is substantially longer for the species with larger kinetic energy. Typically, reflectrons consist of a stack of metal plates linked via a chain of resistors,^{18,31} but the use of a resistive glass tube here allows the reflectron to act as an infinite chain of electrodes. This minimizes lensing and fringe field effects near individual electrodes, in order to maximize the fragment mass resolution of the reflectron, while maintaining its short length. Similar resistive glass tubes have been used in the velocity map imaging of electrons.³³ Once the ions enter the reflectron, the deflector is pulsed (from 0 V to -3 kV, pulse duration ~ 100 μs) to push anions (parent dianions and fragment anions) into the ion detector on the second pass, so that the time-of-flight of each species can be recorded.

If any additional anionic photoproducts are formed following irradiation with laser light, then additional peaks will be observed in the secondary mass spectra. For example, Fl-CO_2^- has a time of flight between Fl^{2-} and Fl^- ($\frac{m}{z} = \frac{330-44}{1} = 286$ amu). Generally, ion

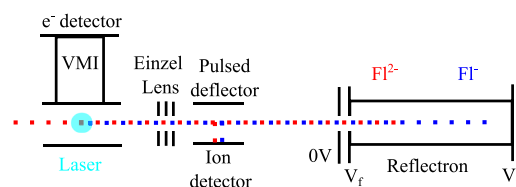


FIG. 1. Schematic of the new detector region including the electron detector, reflectron secondary mass spectrometer, and pulsed ion detection scheme, as used for the experiments on Fl^{2-} . The shorter flight path of Fl^{2-} ($\frac{m}{z} = 165$ amu), produced via electrospray ionization and mass selected from its time-of-flight, is represented by the red dots, whereas the longer flight path of Fl^- ($\frac{m}{z} = 330$ amu) is shown by the blue dots.

peaks are assigned to a specific $\frac{m}{z}$ by comparison of the experimental ion arrival times to the results of a simple model, which calculates the acceleration of an ion of a specific $\frac{m}{z}$ within the applied fields, extracts an ion turn around the position, and ultimately predicts a time-of-flight.

Following the assignment of the species in the secondary mass spectrum, action spectra can be recorded by monitoring the intensity of the signal from a specific mass-selected species, as a function of laser wavelength. The laser was scanned at a rate of 0.1 nm s^{-1} , and the scans were repeated three times. All of the ion peak intensities in the following action spectra were normalized to the integral of the parent dianion peak in order to account for substantial fluctuations in the parent ion beam. The low intensity of the fragment signal requires additional amplification after the detector, resulting in saturation of the Fl^{2-} ion signal on the final time-of-flight trace (Fig. S11). However, the effect of this on the reported action spectra is minimal, as the Fl^{2-} ion intensity was very constant, as verified by measurement of the parent ion signal without further amplification and by repeated measurements of the action spectra, which were very similar. We are currently modifying the data acquisition setup to allow us to independently amplify the fragment signal, which should result in a more sensitive normalization procedure in the future. It should also be noted that no attempt has been made to account for the significant changes in laser intensity, which occur over this wavelength range, with particular minima being observed at 400 and 292 nm, which are characteristic of our optical parametric oscillator, while over other regions, the output was found to be relatively constant in terms of pulse energy. Electron yield spectra can also be acquired by simply monitoring the number of electrons on the imaging detector as a function of wavelength.

To aid the interpretation of the results, additional electronic structure calculations were performed on Fl^{2-} , Fl^- , and Fl-CO_2^- . Ground state density functional theory (DFT) calculations and excited state time-dependent DFT calculations, using the Tamm-Dancoff approximation, were performed using the Gaussian software package at the B3LYP level of theory with the 6-311G++2d,2p basis set.³⁵⁻³⁷

III. RESULTS AND ANALYSIS

In the absence of laser light, the secondary mass spectrum consisted of a single peak with $\frac{m}{z} = 165 \text{ amu}$, assignable to Fl^{2-} . Once the sample was irradiated, two further peaks were observed over specific wavelength ranges, corresponding to Fl-CO_2^- and Fl^{2-} . An example time-of-flight spectrum is shown in the supplementary information, Fig. S11. No evidence was seen for the formation of other products such as Fl-CO_2^{2-} , indicating that dissociation only occurred in conjunction with electron loss.

A. Photoelectron imaging of Fl^{2-}

Previous work in our group has studied the photodetachment dynamics of Fl^{2-} using frequency resolved photoelectron imaging.^{3,12,27} A brief overview of this work is presented here as its conclusions will guide some of the discussion below. Figure 2 shows the Fl^{2-} photoelectron image recorded at $\lambda = 320 \text{ nm}$, where two clear spectral features are observed. Photoelectron imaging in the visible reported a single fixed eKE feature, which remains even in

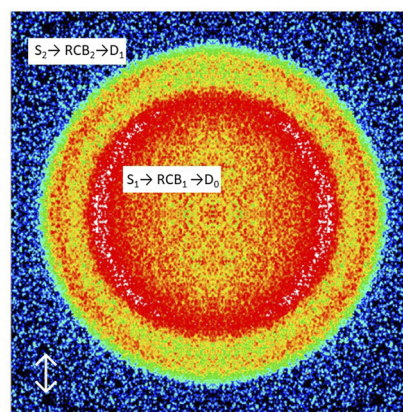


FIG. 2. Raw (symmetrized) photoelectron image of Fl^{2-} recorded at $\lambda = 320 \text{ nm}$ with the polarization vector of the light shown by the double arrow.

the UV and corresponds to the inner ring in Fig. 2. This feature arises from resonant tunneling through an RCB associated with the $\text{Fl}^{2-}[\text{S}_1]$ state (RCB_1).³ As this feature's eKE is fixed with decreasing λ , the excess photon energy following electron loss will be deposited as internal rovibrational energy in the ground-state anion, $\text{Fl}^-[\text{D}_0]$.³ For UV excitation, a second higher-lying and competing tunneling pathway (outer ring in Fig. 2) appears following excitation to the S_2 state of Fl^{2-} , $\text{Fl}^{2-}[\text{S}_2]$. A fraction of the population tunnels through a RCB associated with the S_2 state, RCB_2 , resulting in a different final anion electronic state, $\text{Fl}^-[\text{D}_1]$.¹² The different final states accessed by tunneling arise from different Koopmans' correlations.¹² At wavelengths in the visible ($\lambda \leq 540 \text{ nm}$), only the inner feature is observed in the photoelectron images, whereas the outer ring competes at higher photon energies in the UV ($\lambda \leq 350 \text{ nm}$). In addition, a minor direct detachment channel was observed for $\lambda \leq 440 \text{ nm}$ at electron kinetic energies that overlapped with the resonant tunneling pathway mediated by S_2 (outer ring).

B. Action spectra of Fl^{2-} : Fragment and electron yield

In order to confirm the functionality of the new reflectron, the action spectra of both the electron and Fl^- yield arising from photodetachment of Fl^{2-} were recorded at wavelengths between 400 and 600 nm and are shown in black in Fig. 3. The electron action spectrum is smoothed via a 20-point moving average, with the raw data shown in gray. The electron and Fl^- action spectra are similar in structure, indicating that the primary process following absorption of a photon is a one-photon photodetachment to form the radical anion i.e., $\text{Fl}^{2-} \rightarrow \text{Fl}^- + e^-$, in agreement with previous work.^{2,3} The small differences between the electron and the Fl^- yield spectra, shown in black, are likely to be within the noise of the two measurements or attributable to the two spectra being recorded with different detectors.

The black line in Fig. 4 is the action spectrum of Fl^{2-} recorded over a wider wavelength range, $\lambda = 260\text{--}600 \text{ nm}$, by monitoring the Fl^- fragment. This action spectrum has a similar structure to the previously reported gas-phase action spectrum of Fl^{2-} and the absorption spectrum of Fl^{2-} in water at $\lambda > 400 \text{ nm}$, indicating that

the regions of increased signal intensity are due to the presence of an increased photodetachment cross section for FI^{2-} , i.e., the location of an excited electronic state.^{1,2} The most intense feature is centered around 500 nm and corresponds to the bright $S_0 \rightarrow S_1$ transition in FI^{2-} . This feature shows some vibrational structure, similar to the solution phase absorption spectrum. Irradiation of FI^{2-} near 400 nm produces very little FI^- , indicating that the photodetachment cross section is very low in this region, even though, at this wavelength,

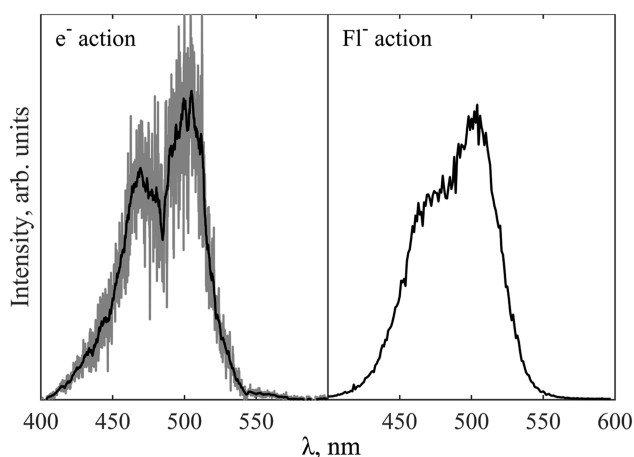


FIG. 3. Comparison of the action spectra of FI^{2-} recorded by monitoring the electron yield on the left (gray and a 20-point moving average in black) and the FI^- yield on the right in black.

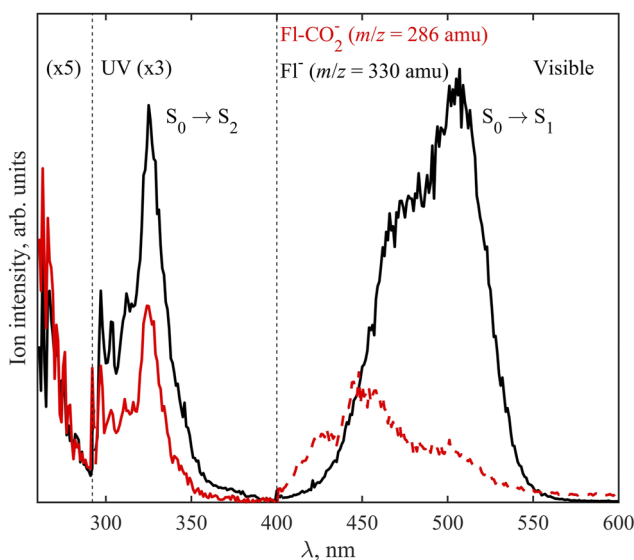


FIG. 4. The action spectra of FI^{2-} obtained by monitoring the fragments FI^- (black) and FI-CO_2^- (red). All the processes are one-photon, except for the dashed line that arises from a multiple photon process (see text for more details). The vertical dashed lines indicate three different spectral ranges of the light source and the relative intensities on either side of these lines are not representative of the true intensity.

direct “over-the-RCB” detachment is an open channel.^{3,12} At higher photon energies, an increased yield of FI^- is observed, as higher-lying electronic states of FI^{2-} become energetically accessible. In particular, S_2 is located near 325 nm, with potential evidence for S_3 at $\lambda < 292$ nm. It should be noted that a portion of this action spectrum ($\lambda = 300\text{--}600$ nm) has been published before.¹²

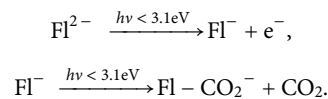
C. Action spectrum of FI^{2-} : FI-CO_2^- yield

The action spectrum of FI^{2-} recorded by monitoring the yield of the decarboxylated anion FI-CO_2^- was also measured using the reflectron and is shown in red in Fig. 4. The FI-CO_2^- yield spectrum is similar in appearance to FI^- at wavelengths shorter than 400 nm (solid red line) but significantly different at longer wavelengths (dashed red line). The excellent correlation between the FI-CO_2^- and FI^- yield spectra for $300 < \lambda < 400$ nm indicates that a one-photon process can either lead to just electron loss or combined electron and CO_2 loss, with the former being approximately twice as likely around the S_2 excited state.

In the visible range, the discrepancy between the FI-CO_2^- and FI^- yield spectra is due to a multiple photon process, which can be evidenced by the action spectrum taken at lower laser power. As the formation of FI^- is a one-photon process, differences in the relative intensity of the FI-CO_2^- peak would indicate a multiple photon process. Figure S12 shows the FI^{2-} action spectra recorded by monitoring the FI^- and FI-CO_2^- yields at wavelengths between 400 and 500 nm and at a third of the laser power used for the measurement in Fig. 4. Based on the large decrease in the relative intensity of FI-CO_2^- compared to FI^- from Fig. 4 to S12, we conclude that the formation of FI-CO_2^- at $\lambda > 400$ nm occurs via a multiple photon process, presumably a two-photon process (dashed red line). The formation of FI^- at all wavelengths and FI-CO_2^- for $\lambda < 400$ nm is a one-photon process (solid red line).

D. Action spectrum of FI^-

The power dependent measurements suggest that electron loss and decarboxylation occur stepwise via a two-photon process at wavelengths longer than 400 nm ($h\nu < 3.1$ eV),



The second step corresponds to the action spectrum of the radical anion FI^- rather than the parent dianion. Hence, the total measured action spectrum of FI^{2-} by monitoring the FI-CO_2^- fragment (red line in Fig. 4) across the visible contains both steps. By scaling the FI^- yield spectrum to fit the red-edge of the FI-CO_2^- yield spectrum and subsequently taking their difference, it is possible to extract the $\text{FI}^-[\text{D}_0]$ action spectrum. The action spectrum of FI^- (blue) as well as the scaled versions of the FI^- (black) and FI-CO_2^- (red) yield spectra are shown in Fig. 5. The action spectrum of FI^- is similar in structure to the action spectrum of FI^{2-} in Fig. 4 (black) but shifted to higher energy. Note also that three peaks are seen with a similar spacing (~ 0.15 eV), suggesting that they correspond to the vibrational manifold of the $\text{FI}^-[\text{S}_1]$ excited state. The low intensity of the lowest energy peak is indicative that this feature may correspond to a hot

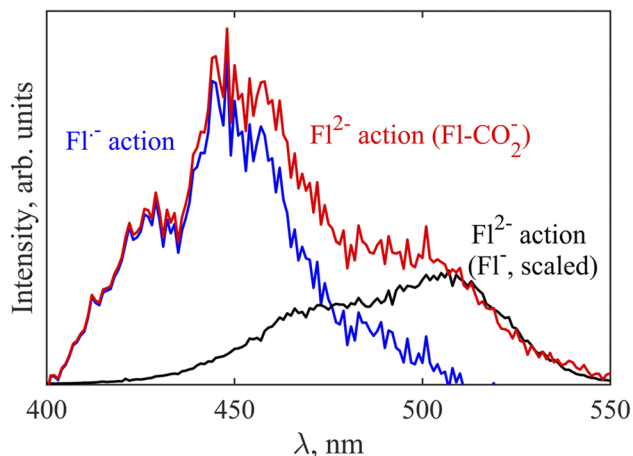


FIG. 5. Action spectrum of the FI^- radical anion (blue) extracted from action spectra of FI^{2-} by taking the difference of the FI-CO_2^- (red) and the scaled FI^- (black) yield spectra.

band, which is unsurprising, given the likely presence of significant internal excitation in the anion following electron loss.³

IV. DISCUSSION

Decarboxylation is a common process in carboxylates and carboxyl radicals, driven by the large thermodynamic stability of CO_2 .^{4,5,38–40} It has been observed to occur via a photodissociation or dissociative photodetachment (DPD) process in carboxylate anions and even via secondary dissociative autodetachment in dicarboxylate dianions.^{4,5,40} In the case of combined electron and CO_2 loss, as observed for FI^{2-} , it is likely that electron loss and CO_2 loss occur sequentially rather than via the formation of CO_2^- , given that CO_2 has a negative electron affinity.⁴¹ Therefore, the mechanism for decarboxylation of FI^{2-} is likely to be either DPD ($\text{FI}^{2-} \xrightarrow{h\nu} \text{FI}^- + \text{CO}_2 + e^-$), which may occur via a repulsive electronic state of the FI^- anion, e.g., $\text{FI}^-[\text{D}_1]$, or via the formation of a vibrationally excited $\text{FI}^-[\text{D}_0]$, which then undergoes unimolecular dissociation or a combination of these processes on different anionic electronic states.

As electron loss is the first step in the formation of both FI^- and FI-CO_2^- , the photoelectron imaging of FI^{2-} (e.g., Fig. 2) will inform on the electron loss processes that lead to specific fragments at a given wavelength (Fig. 4).^{3,12} Two resonant electron loss processes have been observed: (1) resonant tunneling through RCB_1 from the $\text{FI}^{2-}[\text{S}_1]$ to $\text{FI}^-[\text{D}_0]$ at all wavelengths studied ($300 \text{ nm} \leq \lambda \leq 540 \text{ nm}$) and (2) a second resonant tunneling channel through RCB_2 from $\text{FI}^{2-}[\text{S}_2]$ to $\text{FI}^-[\text{D}_1]$ at $\lambda < 350 \text{ nm}$.^{3,12} For $\lambda < 350 \text{ nm}$, both processes compete as both are visible in the photoelectron image (Fig. 2).¹² There is a third electron loss channel due to detachment to $\text{FI}^-[\text{D}_0]$ over RCB_0 (linking $\text{FI}^{2-}[\text{S}_1]$ and $\text{FI}^-[\text{D}_0]$) occurring at $\lambda \leq 440 \text{ nm}$.^{3,42} However, this is a very minor channel as evidenced by the low FI^- ion signal observed at non-resonant wavelengths ($350 \text{ nm} \leq \lambda \leq 440 \text{ nm}$).¹²

At the longest wavelengths studied ($440 \leq \lambda \leq 600 \text{ nm}$), absorption of a single photon populates the excited dianion state, $\text{FI}^{2-}[\text{S}_1]$,

and the only available channel is electron tunneling through RCB_1 to form a $\text{FI}^-[\text{D}_0]$,³ with no decarboxylation. The final anionic product $\text{FI}^-[\text{D}_0]$, while internally hot, is stable on a timescale longer than the flight time ($\sim 20 \mu\text{s}$) as it is observed in the fragment action spectra (Fig. 4).³ At shorter wavelengths ($\lambda \leq 350 \text{ nm}$), where the two resonant electron loss channels compete, there is ion intensity in the FI^- and FI-CO_2^- yield spectra (Fig. 4) in a ratio of $\sim 2:1$, indicating a competition between photodetachment and DPD following one-photon excitation of FI^{2-} . One explanation is that $\text{FI}^-[\text{D}_1]$ is a repulsive electronic state, whereas $\text{FI}^-[\text{D}_0]$ is bound, such that CO_2 loss occurs readily following the formation of $\text{FI}^-[\text{D}_1]$, whereas $\text{FI}^-[\text{D}_0]$ is stable on the timescale of the experiment i.e., the flight time from the interaction region to the turnaround point in the reflectron. Evidence for FI-CO_2^- formation via a repulsive dissociation is found in the comparable width of the FI-CO_2^- and FI^- peaks in the time-of-flight spectrum (Fig. S11). This indicates that the timescale of decarboxylation is shorter than the flight time from the interaction region to the reflectron ($\sim 5 \mu\text{s}$) because if dissociation occurred within the reflectron itself, a much broader distribution of ion arrival times would be expected. Hence, the DPD process appears to be prompt rather than statistical in nature.

In order to investigate the dissociation dynamics further, electronic structure calculations were performed on FI^{2-} , FI^- , and FI-CO_2^- , and the results are shown in Table I. Of most importance to the decarboxylation process is the relative energetics of the $\text{FI}^-[\text{D}_0]$ and $\text{FI}^-[\text{D}_1]$ states compared to the dissociation asymptote $\text{FI-CO}_2^- + \text{CO}_2$. The calculations indicate that $\text{FI}^-[\text{D}_0]$ is bound with respect to $\text{FI-CO}_2^- + \text{CO}_2$, with a bond dissociation energy of 0.82 eV. The calculated bond dissociation energy of $\text{FI}^-[\text{D}_1]$ is much smaller, at 0.09 eV, which may also indicate that $\text{FI}^-[\text{D}_1]$ is bound with respect to CO_2 loss but is within the error of the calculations and comparable to the expected internal energy of anions at 298 K. Regardless, our relative energies show clearly that decarboxylation is more facile in $\text{FI}^-[\text{D}_1]$ than in $\text{FI}^-[\text{D}_0]$.

The larger calculated bond dissociation energy of the $\text{FI}^-[\text{D}_0]$ compared with the $\text{FI}^-[\text{D}_1]$ state, together with the experimental observations of competition between the formation of FI^- and FI-CO_2^- following excitation to S_2 ($\lambda \leq 350 \text{ nm}$), and of a relatively rapid dissociation ($< 5 \mu\text{s}$), are consistent with the conclusion that decarboxylation is favored following resonant tunneling through RCB_2 . Effectively, $\text{FI}^-[\text{D}_1]$ loses CO_2 rapidly, whereas $\text{FI}^-[\text{D}_0]$ is stable on the timescale of the experiment. The negligible bond

TABLE I. Relative energetics of FI^{2-} , FI^- , and FI-CO_2^- in various electronic states. Vertical excitation and detachment energies are labeled VEE and VDE, respectively. Values labeled with an asterisk have been reported previously.¹²

| Species (electronic state) | Relative energy (eV) |
|--------------------------------|----------------------|
| $\text{FI}^{2-}[\text{S}_0]$ | 0* |
| $\text{FI}^-[\text{D}_0]$ | 0.62 (0.74 VDE)* |
| $\text{FI}^-[\text{D}_1]$ | 1.35 (VEE)* |
| $\text{FI-CO}_2^-[\text{D}_0]$ | 1.44 |
| + CO_2 | 1.44 |
| $\text{FI}^{2-}[\text{S}_1]$ | 2.66 (VEE)* |
| $\text{FI}^{2-}[\text{S}_2]$ | 3.01 (VEE)* |

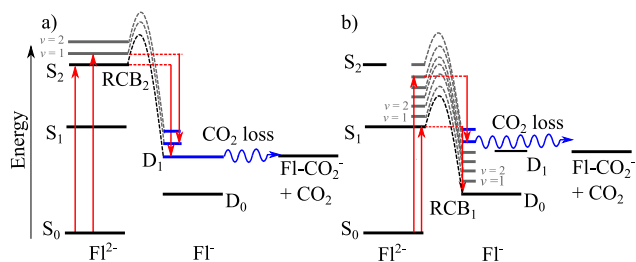


FIG. 6. Cartoon of the possible decarboxylation routes following electron loss via (a) resonant tunneling through RCB_2 and rapid decarboxylation and (b) resonant tunneling through RCB_1 and slow decarboxylation for highly internally excited anions. Electronic dynamics (including photoexcitation) are shown in red with CO_2 decarboxylation dynamics in blue. Vibrational energy levels of D_0 and D_1 with sufficient energy for decarboxylation are also shown in blue.

dissociation energy for $\text{FI}^-[\text{D}_1]$ suggests that loss of CO_2 is energetically possible whenever $\text{FI}^{2-}[\text{S}_2]$ can be excited, which matches well with the observed action spectra where one-photon decarboxylation is seen for $\lambda < 350$ nm and suggests that the potential energy surface would be, at most, weakly repulsive. A cartoon illustrating the rapid decarboxylation of $\text{FI}^-[\text{D}_1]$, following its formation via tunneling through RCB_2 , is shown in Fig. 6(a).

However, if the above picture of dissociation was complete, we would expect to see a fixed ratio of FI^- and FI-CO_2^- once excitation to $\text{FI}^{2-}[\text{S}_2]$ was energetically accessible. In reality, the relative intensity of the FI-CO_2^- signal compared to FI^- increases with photon energy, as shown in Fig. S13, suggesting that there is a second dissociation mechanism at play. As we have established that decarboxylation must follow electron loss via tunneling through a RCB, we conclude that one-photon DPD must also be a possible channel from $\text{FI}^-[\text{D}_0]$ when sufficient vibrational energy is present to overcome the bond dissociation energy. The $\text{FI}^-[\text{D}_0]$ state is populated following resonant electron loss from $\text{FI}^{2-}[\text{S}_1]$ and so decarboxylation becomes energetically accessible for $\lambda < 375$ nm, corresponding to the energy of $\text{FI}^{2-}[\text{S}_1]$ plus the $\text{FI}^-[\text{D}_0]$ dissociation energy [2.48 eV (500 nm) + 0.82 eV = 3.30 eV (375 nm)]. This decarboxylation channel, shown in Fig. 6(b), would be expected to increase in favourability as the photon energy increases because there is a larger likelihood of the vibrational modes relevant to decarboxylation to be populated. This decarboxylation mechanism is likely to be slower than dissociation via $\text{FI}^-[\text{D}_1]$ and may be expected to result in a broader time-of-flight distribution for FI-CO_2^- . However, low absolute signal levels make measurement of such broadened features (in a minor channel) not presently feasible, and it should be noted that a prompt (i.e., $< 5 \mu\text{s}$) contribution is also present because it appears in the FI-CO_2^- signal.

In summary, one-photon decarboxylation occurs after excitation to the $\text{FI}^{2-}[\text{S}_2]$, primarily from $\text{FI}^-[\text{D}_1]$ produced via resonant tunneling through RCB_2 , but with a minor contribution from vibrationally excited anions produced via internal conversion from $\text{FI}^{2-}[\text{S}_2]$ to $\text{FI}^{2-}[\text{S}_1]$ and subsequent resonant tunneling through RCB_1 . The combination of these two mechanisms explains the observed one-photon FI^{2-} action spectra when combined with our knowledge of the electron dynamics from photoelectron imaging. This picture of the decarboxylation dynamics is summarized in Fig. 6, which provides a comprehensive view of the possible

mechanisms at play following photoexcitation. This picture is also consistent with the observations from previous CID and IR excitation experiments, where those excitation methods provided sufficient energy to surpass the $\text{FI}^-[\text{D}_0]$ dissociation barrier after an electron has been lost.²

The final consideration is the mechanism of the two-photon electron loss and decarboxylation process, which occurs in the visible region. For $\lambda \geq 400$ nm (Fig. 4), electron loss results in the production of $\text{FI}^-[\text{D}_0]$. The subsequent absorption of a second photon, which results in decarboxylation, is likely to form an electronically excited $\text{FI}^-[\text{D}_n]$. This is supported by the observation of clear vibrational structure in the action spectrum of FI^- (Fig. 5). The $\text{FI}^-[\text{D}_n]$ electronically excited state is higher lying than the $\text{FI}^-[\text{D}_1]$ state, which lies 0.73 eV above $\text{FI}^-[\text{D}_0]$ (see Table I) and may be dissociative along the CO_2 coordinate. Alternatively, decarboxylation could take place following internal conversion to the weakly bound $\text{FI}^-[\text{D}_1]$ state or from the $\text{FI}^-[\text{D}_0]$, although this would be a statistical and slower dissociation mechanism.

V. CONCLUSIONS

A new reflectron secondary mass spectrometer has been used to record the action spectra of the photodetachment and DPD product channels, following irradiation of FI^{2-} at wavelengths between 260 and 600 nm. The action spectrum of FI^{2-} , recorded by monitoring FI^- , indicates that at least two excited states of FI^{2-} are observed. In addition, photoelectron imaging demonstrates the presence of electron loss via several distinct resonant tunneling channels through different RCBs. For $\lambda > 400$ nm, excitation to the $\text{FI}^{2-}[\text{S}_1]$ results in photodetachment, with CO_2 loss only occurring via a two-photon process of photodetachment and subsequent decarboxylation of FI^- . For $\lambda < 400$ nm, CO_2 loss occurs via a one photon process, with increasing relative yields of FI-CO_2^- as the photon energy increases. In addition, electronic structure calculations indicate that $\text{FI}^-[\text{D}_0]$ is bound with respect to decarboxylation, whereas $\text{FI}^-[\text{D}_1]$ is similar in energy to the dissociation asymptote. Taken together, these observations indicate that decarboxylation occurs rapidly following tunneling through RCB_2 and the formation of a $\text{FI}^-[\text{D}_1]$, with a smaller contribution from the formation of highly vibrationally excited $\text{FI}^-[\text{D}_0]$ following tunneling through RCB_1 . Finally, the two-photon process of electron loss via direct detachment or tunneling through RCB_1 and subsequent decarboxylation, which is observed in the visible region, is likely mediated by a high-lying repulsive state of FI^- .

SUPPLEMENTARY MATERIAL

The [supplementary material](#) contains an example time-of-flight trace, a low laser power fragment action spectrum of FI^{2-} , and a plot showing the proportion of decarboxylation as a function of wavelength.

ACKNOWLEDGMENTS

Jemma A. Gibbard is thankful for the support of a Ramsay Memorial Fellowship. The authors would like to thank Adam Mendoza for developing the data acquisition program used to record the action spectra in this work.

AUTHOR DECLARATIONS

Conflict of Interest

The authors have no conflicts to disclose.

Author Contributions

Jemma A. Gibbard: Conceptualization (equal); Formal analysis (lead); Investigation (lead); Writing – original draft (lead); Writing – review & editing (equal). **Jan R. R. Verlet:** Conceptualization (equal); Writing – review & editing (equal).

DATA AVAILABILITY

The data that support the findings of this study are openly in Zenodo at <https://doi.org/10.5281/zenodo.7828814>, Ref. 43.

REFERENCES

- 1 A. Earp, C. E. Hanson, P. J. Ralph, V. E. Brando, S. Allen, M. Baird, L. Clementson, P. Daniel, A. G. Dekker, P. R. C. S. Fearn, J. Parslow, P. G. Stratton, P. A. Thompson, M. Underwood, S. Weeks, and M. A. Doblin, "Review of fluorescent standards for calibration of *in situ* fluorimeters: Recommendations applied in coastal and ocean observing programs," *Opt. Express* **19**(27), 26768–26782 (2011).
- 2 P. D. McQueen, S. Sagoo, H. Yao, and R. A. Jockusch, "On the intrinsic photophysics of fluorescein," *Angew. Chem., Int. Ed.* **49**(48), 9193–9196 (2010).
- 3 D. A. Horke, A. S. Chatterley, and J. R. R. Verlet, "Effect of internal energy on the repulsive Coulomb barrier of polyanions," *Phys. Rev. Lett.* **108**(8), 083003 (2012).
- 4 G. A. Pino, R. A. Jara-Toro, J. P. Aranguren-Abrate, C. Dedonder-Lardeux, and C. Jouvet, "Dissociative photodetachment vs photodissociation of aromatic carboxylates: The benzoate and naphthoate anions," *Phys. Chem. Chem. Phys.* **21**(4), 1797–1804 (2019).
- 5 J. A. Gibbard and R. E. Continetti, "Photoelectron photofragment coincidence spectroscopy of carboxylates," *RSC Adv.* **11**(54), 34250–34261 (2021).
- 6 A. Dreuw and L. S. Cederbaum, "Nature of the repulsive Coulomb barrier in multiply charged negative ions," *Phys. Rev. A* **63**(1), 049904 (2000).
- 7 M. K. Scheller, R. N. Compton, and L. S. Cederbaum, "Gas-phase multiply charged anions," *Science* **270**(5239), 1160–1166 (1995).
- 8 A. Dreuw and L. S. Cederbaum, "Multiply charged anions in the gas phase," *Chem. Rev.* **102**(1), 181–200 (2002).
- 9 J. Kalcher and A. F. Sax, "Gas phase stabilities of small anions: Theory and experiment in cooperation," *Chem. Rev.* **94**(8), 2291–2318 (1994).
- 10 A. I. Boldyrev, M. Gutowski, and J. Simons, "Small multiply charged anions as building blocks in chemistry," *Acc. Chem. Res.* **29**(10), 497–502 (1996).
- 11 J. Simons, "Molecular anions," *J. Phys. Chem. A* **112**(29), 6401–6511 (2008).
- 12 J. A. Gibbard and J. R. R. Verlet, "Kasha's rule and Koopmans' correlations for electron tunnelling through repulsive Coulomb barriers in a polyanion," *J. Phys. Chem. Lett.* **13**(33), 7797–7801 (2022).
- 13 W. E. Boxford, J. K. Pearce, and C. E. H. Dessent, "Ionic fragmentation vs electron detachment in isolated transition metal complex dianions," *Chem. Phys. Lett.* **399**(4), 465–470 (2004).
- 14 P. Weis, O. Hampe, S. Gilb, and M. M. Kappes, "Metastability of isolated platinum and palladium tetrahalide dianions and the role of electron tunneling," *Chem. Phys. Lett.* **321**(5–6), 426–432 (2000).
- 15 P. D. Dau, H.-T. Liu, J.-P. Yang, M.-O. Winghart, T. J. A. Wolf, A.-N. Unterreiner, P. Weis, Y.-R. Miao, C.-G. Ning, M. M. Kappes *et al.*, "Resonant tunneling through the repulsive Coulomb barrier of a quadruply charged molecular anion," *Phys. Rev. A* **85**(6), 064503 (2012).
- 16 M.-O. Winghart, J.-P. Yang, M. Kühn, A.-N. Unterreiner, T. J. A. Wolf, P. D. Dau, H.-T. Liu, D.-L. Huang, W. Klopfer, L.-S. Wang, and M. M. Kappes, "Electron tunneling from electronically excited states of isolated bisdisulzole-derived trianion chromophores following UV absorption," *Phys. Chem. Chem. Phys.* **15**(18), 6726 (2013).
- 17 M.-O. Winghart, J.-P. Yang, M. Vonderach, A.-N. Unterreiner, D.-L. Huang, L.-S. Wang, S. Kruppa, C. Riehn, and M. M. Kappes, "Time-resolved photoelectron spectroscopy of a dinuclear Pt(II) complex: Tunneling autodetachment from both singlet and triplet excited states of a molecular dianion," *J. Chem. Phys.* **144**(5), 054305 (2016).
- 18 J. C. Marcum and J. M. Weber, "Electronic photodissociation spectra and decay pathways of gas-phase IrBr_6^{2-} ," *J. Chem. Phys.* **131**(19), 194309 (2009).
- 19 J. R. R. Verlet, D. A. Horke, and A. S. Chatterley, "Excited states of multiply-charged anions probed by photoelectron imaging: Riding the repulsive Coulomb barrier," *Phys. Chem. Chem. Phys.* **16**(29), 15043–15052 (2014).
- 20 X.-B. Wang and L.-S. Wang, "Photoelectron spectroscopy of multiply charged anions," *Annu. Rev. Phys. Chem.* **60**(1), 105–126 (2009).
- 21 X.-B. Wang, C.-F. Ding, and L.-S. Wang, "Photodetachment spectroscopy of a doubly charged anion: Direct observation of the repulsive Coulomb barrier," *Phys. Rev. Lett.* **81**(16), 3351–3354 (1998).
- 22 L.-S. Wang, C.-F. Ding, X.-B. Wang, and J. B. Nicholas, "Probing the potential barriers and intramolecular electrostatic interactions in free doubly charged anions," *Phys. Rev. Lett.* **81**(13), 2667–2670 (1998).
- 23 J. A. Gibbard, C. J. Clarke, and J. R. R. Verlet, "Photoelectron spectroscopy of the protoporphyrin IX dianion," *Phys. Chem. Chem. Phys.* **23**(34), 18425–18431 (2021).
- 24 W. E. Boxford, M. O. A. El Ghazaly, C. E. H. Dessent, and S. Brøndsted Nielsen, "High-energy collision induced dissociation of iridium hexa-halide dianions: Observation of triple electron detachment and other decay pathways," *Int. J. Mass Spectrom.* **244**(1), 60–64 (2005).
- 25 J. Friedrich, S. Gilb, O. T. Ehrler, A. Behrendt, and M. M. Kappes, "Electronic photodissociation spectroscopy of isolated IrX_6^{2-} ($X = \text{Cl}, \text{Br}$)," *J. Chem. Phys.* **117**(6), 2635–2644 (2002).
- 26 J. C. Marcum, A. Halevi, and J. M. Weber, "Photodamage to isolated mononucleotides—Photodissociation spectra and fragment channels," *Phys. Chem. Chem. Phys.* **11**(11), 1740 (2009).
- 27 C. S. Anstöter, J. N. Bull, and J. R. R. Verlet, "Ultrafast dynamics of temporary anions probed through the prism of photodetachment," *Int. Rev. Phys. Chem.* **35**(4), 509–538 (2016).
- 28 J. A. Gibbard, E. Castracane, A. J. Shin, and R. E. Continetti, "Dissociative photodetachment dynamics of the oxalate monoanion," *Phys. Chem. Chem. Phys.* **22**(3), 1427–1436 (2020).
- 29 Z. Lu and R. E. Continetti, "Dynamics of the acetyloxyl radical studied by dissociative photodetachment of the acetate anion," *J. Phys. Chem. A* **108**(45), 9962–9969 (2004).
- 30 J. A. Gibbard, E. Castracane, A. I. Krylov, and R. E. Continetti, "Photoelectron photofragment coincidence spectroscopy of aromatic carboxylates: Benzoate and *p*-coumarate," *Phys. Chem. Chem. Phys.* **23**(34), 18414–18424 (2021).
- 31 U. Boesl, R. Weinkauff, and E. W. Schlag, "Reflectron time-of-flight mass spectrometry and laser excitation for the analysis of neutrals, ionized molecules and secondary fragments," *Int. J. Mass Spectrom. Ion Processes* **112**(2), 121–166 (1992).
- 32 C. E. H. Dessent and M. A. Johnson, "Photoinitiation of gas-phase S_2N_2 reactions through the Evans–Polanyi excited state surface," *J. Am. Chem. Soc.* **119**(21), 5067–5068 (1997).
- 33 J. Lecoindre, G. M. Roberts, D. A. Horke, and J. R. R. Verlet, "Ultrafast relaxation dynamics observed through time-resolved photoelectron angular distributions," *J. Phys. Chem. A* **114**(42), 11216–11224 (2010).
- 34 L. H. Stanley, C. S. Anstöter, and J. R. R. Verlet, "Resonances of the anthracenyl anion probed by frequency-resolved photoelectron imaging of collision-induced dissociated anthracene carboxylic acid," *Chem. Sci.* **8**(4), 3054–3061 (2017).
- 35 S. Hirata and M. Head-Gordon, "Time-dependent density functional theory within the Tamm–Dancoff approximation," *Chem. Phys. Lett.* **314**(3), 291–299 (1999).
- 36 R. Krishnan, J. S. Binkley, R. Seeger, and J. A. Pople, "Self-consistent molecular orbital methods. XX. A basis set for correlated wave functions," *J. Chem. Phys.* **72**(1), 650–654 (1980).

- ³⁷M. J. Frisch, G. W. Trucks, H. B. Schlegel, G. E. Scuseria, M. A. Robb, J. R. Cheeseman, G. Scalmani, V. Barone, G. A. Petersson, H. Nakatsuji, X. Li, M. Caricato, A. V. Marenich, J. Bloino, B. G. Janesko, R. Gomperts, B. Mennucci, H. P. Hratchian, J. V. Ortiz, A. F. Izmaylov, J. L. Sonnenberg, Williams, F. Ding, F. Lipparini, F. Egidi, J. Goings, B. Peng, A. Petrone, T. Henderson, D. Ranasinghe, V. G. Zakrzewski, J. Gao, N. Rega, G. Zheng, W. Liang, M. Hada, M. Ehara, K. Toyota, R. Fukuda, J. Hasegawa, M. Ishida, T. Nakajima, Y. Honda, O. Kitao, H. Nakai, T. Vreven, K. Throssell, J. A. Montgomery, Jr., J. E. Peralta, F. Ogliaro, M. J. Bearpark, J. J. Heyd, E. N. Brothers, K. N. Kudin, V. N. Staroverov, T. A. Keith, R. Kobayashi, J. Normand, K. Raghavachari, A. P. Rendell, J. C. Burant, S. S. Iyengar, J. Tomasi, M. Cossi, J. M. Millam, M. Klene, C. Adamo, R. Cammi, J. W. Ochterski, R. L. Martin, K. Morokuma, O. Farkas, J. B. Foresman, and D. J. Fox, Gaussian 16 Rev. C.01, Wallingford, CT, 2016.
- ³⁸C. W. West, J. N. Bull, and J. R. R. Verlet, "Charged particle imaging of the deprotonated octatrienoic acid anion: Evidence for a photoinduced cyclization reaction," *J. Phys. Chem. Lett.* **7**(22), 4635–4640 (2016).
- ³⁹L. Lammich, J. Rajput, and L. H. Andersen, "Photodissociation pathways of gas-phase photoactive yellow protein chromophores," *Phys. Rev. E* **78**(5), 051916 (2008).
- ⁴⁰X.-P. Xing, X.-B. Wang, and L.-S. Wang, "Photoelectron imaging of doubly charged anions, $^{-}O_2C(CH_2)_nCO_2^{-}$ ($n = 2-8$): Observation of near 0 eV electrons due to secondary dissociative autodetachment," *J. Phys. Chem. A* **114**(13), 4524–4530 (2010).
- ⁴¹R. N. Compton, P. W. Reinhardt, and C. D. Cooper, "Collisional ionization of Na, K, and Cs by CO₂, COS, and CS₂: Molecular electron affinities," *J. Chem. Phys.* **63**(9), 3821 (1975).
- ⁴²K. Veys and D. Escudero, "Anti-Kasha fluorescence in molecular entities: The central role of the electron-vibrational coupling," *Acc. Chem. Res.* **55**(18), 2698–2707 (2022).
- ⁴³J. A. Gibbard and J. R. R. Verlet (2023). "Unraveling the decarboxylation dynamics of the fluorescein dianion with fragment action spectroscopy," Zenodo. <https://doi.org/10.5281/zenodo.7828814>